

Dark matter effect on the weak deflection angle by black holes at the center of Milky Way and M87 galaxies

Reggie C. Pantig^{1,*} and Ali Övgün^{2,†}

¹*Physics Department, De La Salle University, 2401 Taft Avenue, Manila, 1004 Philippines*

²*Physics Department, Eastern Mediterranean University, Famagusta, 99628 North Cyprus via Mersin 10, Turkey*

In this paper, we investigated the effect of dark matter on the weak deflection angle by black holes at the galactic center. We consider three known dark matter density profiles such as the Cold Dark Matter (CDM), Scalar Field Dark Matter (SFDM), and the Universal Rotation Curve (URC) from the Burkert profile. To achieve this goal, we used how the positional angles are measured by Ishihara et al. method based on Gauss-Bonnet theorem (GBT) on the optical metric. With the help of the non-asymptotic form of the GBT, the longitudinal angle difference is also calculated. First, we find the emergence of apparent divergent terms on the said profiles, which indicates that the spacetime describing the black hole-dark matter combination is non-asymptotic. We showed that these apparent divergent terms vanish when the distance of the source and receiver are astronomically distant from the black hole. Using the current observational data in the Milky Way and M87 galaxies, we find interesting behaviors of how the weak deflection angle varies with the impact parameter, which gives us some hint on how dark matter interacts with the null particles for each dark matter density profile. We conclude that since these deviations are evident near the dark matter core radius, the weak deflection angle offers a better alternative for dark matter detection than using the deviation from the black hole shadow. With the DM profiles explored in this study, we find that SFDM is the most difficult to detect, while the easiest is the URC profile.

PACS numbers: 95.30.Sf, 98.62.Sb, 97.60.Lf

Keywords: Weak gravitational lensing; Black holes; Deflection angle; Gauss-Bonnet theorem; Dark matter.

I. INTRODUCTION

Several decades ago, the existence of a black hole was a mystery and only was explored as a mathematical construct [1]. Until recently, the Event Horizon Telescope collaboration unveiled the first image of the shadow of a black hole in the electromagnetic regime [2–4], which again confirmed the correctness of Einstein’s General Theory of Relativity [5] as a model for compact objects with an extreme gravitational field. With the only confirmation of black hole’s physical existence, one can not underestimate the progress of theoretical research on the search for the most realistic model of a black hole, as well as its dynamical interactions to any astrophysical environments [6–18].

There are recent studies on this specific direction, using perhaps the most important yet mysterious astrophysical environment - the dark matter. Dark matter constitutes about 85% of the total mass of the Universe [19] and is used to explain the strange behavior of stars and galaxy dynamics. At this time of writing, dark matter particles called Weakly Interacting Massive Particles (WIMPs) remain elusive to Earth-based direct detection experiments. Although there was some positive result reported [20–22], it was later criticized due to the null results from other improved direct-detection experiments [23–25]. Thus, from the theoretical perspective at least, one must find an alternative for dark matter detection. Recently, it was proposed that the Earth’s crust itself contains millions of years of data and can act as a huge dark matter detector [26]. Meanwhile, can we also consider an extreme object such as a black hole to detect imprints of dark matter? Numerous research studies recently appeared to explore such a possibility. There are black hole models that came from the solution of the Einstein field equation that includes dark matter. See for example Refs. [27, 28] where the authors considered a perfect fluid dark matter. Dark matter toy models are also considered in studying its effect to the shadow [29, 30], weak deflection angle [31, 32], and the intensity of electromagnetic flux radiation [33]. Until recently, a method was formulated to extract a particular black hole metric combined with some known dark matter profiles, thus, modeling a realistic scenario of a supermassive black hole at the heart of a galaxy surrounded with dark matter [34].

Gibbons and Werner showed a new geometrical technique to calculate the weak deflection angle using the Gauss-Bonnet theorem (GBT) on the optical geometries for asymptotically flat spacetimes [35]. In this method, one can solve the integral of GBT in an infinite domain bounded by the light ray. Then, Werner extended this method to stationary spacetimes by employing the Finsler-Randers type optical geometry with Nazms osculating Riemannian manifolds [36]. Afterward, Ishihara et al. extended this method for finite-distances (huge impact parameter) instead of using the asymptotic receiver and source [37, 38]. Next, T.

*Electronic address: reggie.pantig@dlsu.edu.ph

†Electronic address: ali.ovgun@emu.edu.tr; URL: <https://www.aovgun.com>

Ono et al. applied the finite-distances method to the axisymmetric spacetimes [39]. Crisnejo and Gallo [40] used the GBT to obtain the gravitational deflections of light in a plasma medium. Recently, Li et al. studied the finite-distance effects on weak deflection angle by using massive particles and Jacobi-Maupertuis Randers-Finsler metric within GBT [41–47]. For more recent works, one can see [41–106].

A common result emerges from the aforementioned studies: dark matter is still very difficult to detect through the deviation arising from its effect, say, on the shadow radius of a black hole. In Ref. [107], it was stated that the dark matter effect on the shadow only occurs when its mass k is around 10^7 orders of magnitude, which means the dark matter distribution must be concentrated near the black hole and comparable to the black hole's mass. The study also suggested more improvement on the current resolution capabilities of modern telescopes. The same conclusion was found in Ref. [29, 30, 34, 108]. Even with the consideration of the baryonic matter or the available observational data for the dark matter spike density, little and indistinguishable effect was seen in the black hole shadow [109–111]. In this work, we will calculate the weak deflection angle by black holes lurking at the center of galaxies and determine if we can use such a phenomenon for better dark matter detection. In particular, we will derive the weak deflection angle for a black hole surrounded by known dark matter profiles such as the Cold Dark Matter, Scalar Field Dark Matter [34, 107], and Universal Rotation Curve [108]. The metric of these black holes was derived using the formalism pioneered by Xu et al. in Ref. [34]. The derived spacetime metrics are usually formidable in their exact form but these still satisfy the weak and strong energy conditions which indicate their physicality. See for example [112, 113]. With Xu et al. formalism, these black hole-dark matter metrics are rather new and to the best of our knowledge, there are no existing studies on calculating its weak deflection angle. There are existing studies, however, about other black hole-dark matter models and the calculation of their weak deflection angle and gravitational lensing effects [28, 31, 32, 94, 114–117].

The paper is organized as follows: Sect. II introduces the Ishihara et al. method in calculating the weak deflection angle with the use of the positional and longitudinal angles. In the subsections that follow, the weak deflection angles of black holes with dark matter profiles are derived and discussed. In Sect. III we state concluding remarks and include research prospects. Throughout the paper, we used the natural units $G = c = 1$ and the metric signature $(-, +, +, +)$.

II. WEAK DEFLECTION ANGLE BY GAUSS-BONNET THEOREM AND ISHIHARA-LI METHOD FOR FINITE DISTANCE

Let us consider a non-rotating black hole whose spacetime in its vicinity is described as static and spherically symmetric:

$$ds^2 = -A(r)dt^2 + B(r)dr^2 + C(r)d\theta^2 + D(r)d\phi^2, \quad (1)$$

where $B(r) = A(r)^{-1}$, $C(r) = r^2$, and $D(r) = r^2 \sin^2 \theta$. In studying the weak deflection angle, light rays are important and they satisfy the null condition that $ds^2 = 0$. The optical metric can then be obtained via $dt = \sqrt{\gamma_{ij} dx^i dx^j}$, where γ_{ij} is the spacial curve that runs from 1 to 3. With the optical metric, one can use it alongside with the Gauss-Bonnet theorem [118, 119] which states that

$$\iint_D K dS + \sum_{a=1}^N \int_{\partial D_a} \kappa_g dl + \sum_{a=1}^N \theta_a = 2\pi \quad (2)$$

to study deflection angles. Here, D is any freely orientable 2D curved surface described by the Gaussian curvature K , and dS is the its area element. The boundaries of D are denoted by ∂D_a ($a=1, 2, \dots, N$) with the geodesic κ_g integrated over the line element dl . Furthermore, θ_a and ε_a are the jump and interior angles respectively. See Fig. 1.

When the GBT is applied to a non-rotating black hole where the spacetime metric is asymptotically flat, Ishihara et al. [37] have shown that the weak deflection angle can be found by using the formula

$$\hat{\alpha} = \phi_{RS} + \Psi_R - \Psi_S = - \iint_{\infty_R \square_S^\infty} K dS. \quad (3)$$

Here, Ψ_R and Ψ_S are the angles at the location of the receiver R and the source S respectively, and ϕ_{RS} is the coordinate separation angle between the receiver and the source, which is equal to the difference between the longitudes ϕ_R and ϕ_S . It is further shown in Eq. (3) how these angles are related to the GBT where the Gaussian optical curvature $K = \frac{R_r \phi_r \phi}{\gamma}$ is integrated over the quadrilateral $\infty_R \square_S^\infty$. Here, γ is defined as the determinant of the optical metric γ_{ij} . Ishihara et al. [37] also proved that when the finite distances of the source and the receiver are considered, the LHS of the Eq. (3) is equivalent to

$$\hat{\alpha} = \int_{u_R}^{u_o} \frac{1}{\sqrt{F(u)}} du + \int_{u_S}^{u_o} \frac{1}{\sqrt{F(u)}} du + \Psi_R - \Psi_S, \quad (4)$$

where it is clear how ϕ_{RS} should be calculated. Here, $F(u)$ is the orbit equation expressed in terms of the inverse r -coordinate (ie. $r = 1/u$):

$$\left(\frac{du}{d\phi} \right)^2 \equiv F(u) = \frac{u^4}{b^2} \frac{D(u)(D(u) - A(u)b^2)}{A(u)B(u)}. \quad (5)$$

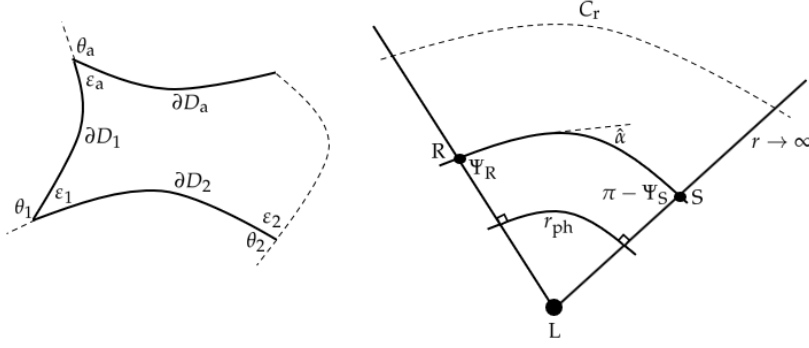


FIG. 1: In the left is the schematic picture of a curved surface for Gauss-Bonnet theorem. In the right, the upper quadrilateral describes the domain for GBT as found by Ishihara et al. [37], while the middle quadrilateral was used in Ref. [45] for non-asymptotic spacetimes.

The upper integration limit u_o in Eq. (4) is the iterative solution to Eq. (5) while the boundary condition $\frac{du}{d\phi}|_{\phi=\frac{\pi}{2}} = 0$ is imposed. Eq. (4) is an elegant equation, handling non-asymptotically flat spacetimes where Eq. (3) fails to work. An example would be those metrics that involve the cosmological constant, or those that have r and r^2 terms in the metric function.

Recently, the study conducted in Ref. [45] also managed to use the GBT to calculate the weak deflection angle of non-asymptotically flat spacetimes. To do so, they used the middle quadrilateral in Fig. 1 which involves the photon radius, or in general, the circular orbit of a time-like particle. In their formalism, the weak deflection angle can be calculated using

$$\hat{\alpha} = \phi_{RS} + \Psi_R - \Psi_S = \iint_{R_{r_{co}} \square_S^{r_{co}}} K dS + \phi_{RS}, \quad (6)$$

where r_{co} is replaced by r_{ph} for photon deflection angle. The interested reader is invited to look on Ref. [45] for the complete treatment of their method and applications.

Now based on observing Eqs. (3) and (6), it occurs that it is easier to calculate the weak deflection angle by using the original definition of $\hat{\alpha} = \phi_{RS} + \Psi_R - \Psi_S$ since it avoids the task of integrating a particular expression for the Gaussian optical curvature. As we know, metric functions that contain simple expressions are easy to calculate using the GBT, especially if these functions are derived as a solution to the Einstein field equation. However, there exist some metric functions that are complicated enough that integrating their Gaussian optical curvature, or by integrating the inverse-root of the orbit equation, gives no analytical expression or very complicated results. Examples of these metrics are the ones derived using Xu et al. [34] formalism that involves a black hole surrounded by dark matter described by a density profile. See Refs. [112, 113] for example, and the one recently derived by Jusufi et al. [107–111].

In this paper, since we are interested in deriving the weak deflection angles by black holes at the center of a galaxy surrounded by dark matter, we will avoid such integrals in the expressions in Eqs. (3) and (6). Instead, we will focus on the calculation of the positional angles Ψ and longitudinal angle ϕ . We can calculate Ψ by going back to Eq. (3), where the angles Ψ_R and Ψ_S , $\cos \Psi \equiv \gamma_{ij} e^i R^j$ can be defined using the inner product of the unit basis vector e^i along the equatorial plane, and the unit radial vector R^i with relative to the lensing object [37]: ie.

$$e^i = \left(\frac{dr}{dt}, 0, \frac{d\phi}{dt} \right) = \frac{d\phi}{dt} \left(\frac{dr}{d\phi}, 0, 1 \right)$$

$$R^i = \left(\frac{1}{\sqrt{\gamma_{rr}}}, 0, 0 \right). \quad (7)$$

By using the orbit equation $F(r)$, $\cos \Psi$ can be recasted as

$$\sin \Psi = \sqrt{\frac{A(r)}{D(r)}} b \quad (8)$$

which is more convenient to calculate than $\cos \Psi$. Finally, for the calculation of the longitudinal angle ϕ , it is done by iteratively solving the orbit equation in Eq. (5) [85].

A. Effect of the CDM profile on weak deflection angle by black holes

The Cold Dark Matter density profile is one of the most well-known profile that is consistent with astronomical observations in the large scale [120, 121]. Although the physical nature of dark matter is unknown, dark matter particles are modeled with non-relativistic motion. The CDM density profile is expressed

$$\rho = \frac{\rho_c}{\frac{r}{r_c} \left(1 + \frac{r}{r_c}\right)^2}, \quad (9)$$

where ρ is the Universe's density at the time of dark matter collapse, while ρ_c and r_c are the core density and radius respectively. It is shown in [34] how we can obtain the black hole metric function with the CDM profile associated with Eq.(9). First, the mass profile for the dark matter halo is calculated as

$$M_{DM}(r) = 4\pi \int_0^r \rho(r') r'^2 dr'. \quad (10)$$

Then using the mass profile, the tangential velocity of test particle in dark matter halo is calculated easily by $v_{tg}^2(r) = M_{DM}(r)/r$. On the other hand, if the line element describing the dark matter halo is given by

$$ds^2 = -f(r)dt^2 + f(r)^{-1}dr^2 + r^2d\theta^2 + r^2 \sin^2 \theta d\phi^2, \quad (11)$$

we can derive a rotational velocity of a test particle in static and spherical symmetric space-time using the relation

$$v_{tg}^2(r) = \frac{r}{\sqrt{f(r)}} \frac{d\sqrt{f(r)}}{dr} = r \frac{d \ln(\sqrt{f(r)})}{dr}. \quad (12)$$

See [34] for details. Now, using the above relations for the rotation velocities, the metric function can be derived by using:

$$f(r) = \exp \left[2 \int \frac{v_{tg}^2(r)}{r} dr \right], \quad (13)$$

and one finds

$$A(r) = \left(1 + \frac{r}{r_c}\right)^{-\frac{8\pi k}{r}} - \frac{2m}{r}. \quad (14)$$

Here, we denote k in $A(r)$ as the dark matter mass given by $k = \rho_c r_c^3$.

The orbit equation $F(u)$ can then be easily calculated using Eq. (5) as

$$F(u) = \frac{1}{b^2} - u^2 + 2mu^3 + 8\pi u^3 k \ln \left(\frac{1}{ur_c} \right), \quad (15)$$

where the first three terms are the known orbit equation for the Schwarzschild case and the last term is the dark matter contribution. We then obtain the distance of closest approach by solving $F(u)$ iteratively:

$$u_o = \frac{\sin \phi}{b} + \frac{m(1 + \cos^2 \phi)}{b^2} + \frac{4\pi k \left[(b + 3m) \ln \left(\frac{b}{r_c} \right) - m \right]}{b^2(b - 2m)}. \quad (16)$$

Using this, we can solve the angle ϕ directly. We then obtained

$$\begin{aligned} \phi_{RS} = & (\phi_{RS})_{Schw} + \frac{4\pi k}{b} \ln \left(\frac{b}{r_c} \right) \left[\frac{1}{\sqrt{1 - b^2 u_R^2}} + \frac{1}{\sqrt{1 - b^2 u_S^2}} \right] \\ & - \frac{4\pi k m}{b^2} \left\{ \frac{\left[1 - b^2 u_R^2 + (b^3 u_R^3 + 5b^2 u_R^2 - 5) \ln \left(\frac{b}{r_c} \right) \right]}{(1 - b^2 u_R^2)^{3/2}} + \frac{\left[1 - b^2 u_S^2 + (b^3 u_S^3 + 5b^2 u_S^2 - 5) \ln \left(\frac{b}{r_c} \right) \right]}{(1 - b^2 u_S^2)^{3/2}} \right\} + \mathcal{O}(m^2, k^2, m^2 k^2), \end{aligned} \quad (17)$$

where, for simplicity, we have written

$$(\phi_{RS})_{\text{Schw}} = \pi - \arcsin bu_R - \arcsin bu_S - \frac{m}{b} \left[\frac{(b^2 u_R^2 - 2)}{\sqrt{1 - b^2 u_R^2}} + \frac{(b^2 u_S^2 - 2)}{\sqrt{1 - b^2 u_S^2}} \right]. \quad (18)$$

Now, using Eq. (8), we have

$$\begin{aligned} \Psi_R - \Psi_S &= (\Psi_R - \Psi_S)_{\text{Schw}} + 4\pi bk \left[\frac{u_R^2 \ln(r_c u_R)}{\sqrt{1 - b^2 u_R^2}} + \frac{u_S^2 \ln(r_c u_S)}{\sqrt{1 - b^2 u_S^2}} \right] \\ &\quad - 4\pi bkm \left[\frac{u_R^3 (2b^2 u_R^2 - 1) \ln(r_c u_R)}{(1 - b^2 u_R^2)^{3/2}} + \frac{u_S^3 (2b^2 u_S^2 - 1) \ln(r_c u_S)}{(1 - b^2 u_S^2)^{3/2}} \right] + \mathcal{O}(m^2, k^2, m^2 k^2), \end{aligned} \quad (19)$$

where

$$(\Psi_R - \Psi_S)_{\text{Schw}} = -\pi + \arcsin bu_R + \arcsin bu_S - bm \left[\frac{u_R^2}{\sqrt{1 - b^2 u_R^2}} + \frac{u_S^2}{\sqrt{1 - b^2 u_S^2}} \right]. \quad (20)$$

Combining the two previous equations above, we obtain the weak deflection angle with finite distance of the source and the receiver as

$$\begin{aligned} \hat{\alpha} &= \frac{2m}{b} \left(\sqrt{1 - b^2 u_R^2} + \sqrt{1 - b^2 u_S^2} \right) + \frac{4\pi k}{b} \left\{ \frac{[b^2 u_R^2 \ln(r_c u_R) + \ln(\frac{r_c}{b})]}{\sqrt{1 - b^2 u_R^2}} + \frac{[b^2 u_S^2 \ln(r_c u_S) + \ln(\frac{r_c}{b})]}{\sqrt{1 - b^2 u_S^2}} \right\} \\ &\quad - \frac{4\pi km}{b^2} \left\{ \frac{u_R^3 b^3 (2b^2 u_R^2 - 1) \ln(r_c u_R)}{(1 - b^2 u_R^2)^{3/2}} + \frac{u_S^3 b^3 (2b^2 u_S^2 - 1) \ln(r_c u_S)}{(1 - b^2 u_S^2)^{3/2}} \right. \\ &\quad \left. + \frac{[(b^3 u_R^3 + 5b^2 u_R^2 - 5) \ln(\frac{b}{r_c}) - b^2 u_R^2 + 1]}{(1 - b^2 u_R^2)^{3/2}} + \frac{[(b^3 u_S^3 + 5b^2 u_S^2 - 5) \ln(\frac{b}{r_c}) - b^2 u_S^2 + 1]}{(1 - b^2 u_S^2)^{3/2}} \right\} + \mathcal{O}(m^2, k^2, m^2 k^2). \end{aligned} \quad (21)$$

We note that this leads to the weak deflection angle $\hat{\alpha} = 4m/b$ in the Schwarzschild case when there is no dark matter mass ($k = 0$) in the far approximation. We can also see in Eq. (21) how the value of u depends on the impact parameter b . For $\hat{\alpha}$ to have some physical significance, u should not be any lower than $1/b$.

In Eq. (21), the quantity $\ln(r_c u)$ is undefined when u is exactly zero. However, if u has a finite value no matter how near it is to zero, there is a certain finite value for $\ln(r_c u)$. Notice also that the u^2 factor dominates the $\ln(r_c u)$ and the whole term can be safely approximated to zero. Hence, assuming that $u_R = u_S$ and are very small, Eq. (21) can still be approximated as

$$\hat{\alpha} = \frac{4m}{b} + \frac{8\pi k}{b} \ln\left(\frac{b}{r_c}\right) + \frac{8\pi km}{b^2} \left[5 \ln\left(\frac{b}{r_c}\right) + 1 \right]. \quad (22)$$

Let us use the available data for Sgr. A* [107] where the values of the dark matter core density and core radius are $\rho_c = 1.936 \times 10^7 M_\odot \text{kpc}^{-3}$ and $r_c = 17.46 \text{ kpc}$ respectively. The dark matter mass is then $k = 1.030 \times 10^{11} M_\odot$ while the black hole mass at the center is $m = 4.30 \times 10^6 M_\odot$. It is useful to express k in terms of the black hole mass unit and this gives $k = 23953m$. Notice that if we compare m to r_c , it is indeed that Eq. (21) applies to the situation. We can still use this equation at the location where the "cusp" phenomenon begins to occur, which is 1 kpc and below. [34, 122]. We note, however, that one cannot use the equation when the impact parameter is very close to the black hole. Thus, a reasonable range for the impact parameter will be shown to demonstrate the effect of the dark matter of various profiles.

Fig. 2 shows the plot of Eq. (21). For comparison, we also plotted the weak deflection angle $\hat{\alpha}$ by the black hole alone, which is so small considering the range for b/m (blue dashed line). When the effect of the CDM profile is taken into account (black solid line), we see some interesting deviations from the Schwarzschild case. When $b \gg r_c$, we can see that the solid black line is asymptotic to the Schwarzschild case. As the impact parameter is getting near the core radius, we see a slight increase in the weak deflection angle, until it decreases again. When $b = r_c$, the dominant term is still the Schwarzschild contribution again. Now, when $b < r_c$ (ie. inside the core radius), we observe repulsive deflection by the black hole due to the effect of the CDM profile. The negative deflection angle increases as b/m continue to decrease. We can also see that the deviation of $\hat{\alpha}$ between the outer core radius and where the cusp began is minuscule in comparison inside the cusp region. We remark that the repulsive deflection angle is nothing new since in [123], the deflection angle due to the black hole in $(2 + 1)\text{D}$ massive gravity also sometimes gives a negative value.

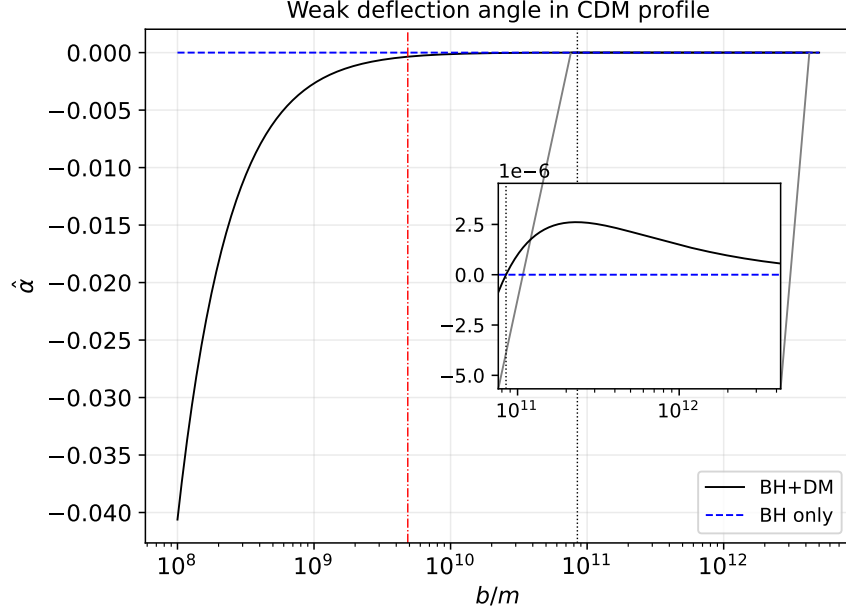


FIG. 2: Curve of the weak deflection angle in the CDM profile for different values of the dimensionless impact parameter b/m . The vertical dotted line is the value of the outermost core radius $r_c \sim 8.484 \times 10^{10} m$. The region below the dash-dotted vertical line is the cusp region ($\sim 4.86 \times 10^9 m$).

B. Effect of the SFDM profile on weak deflection angle by black holes

The CDM profile is known to exhibit a cusp phenomenon near the black hole, around 1 kpc and below in particular. The Scalar Field Dark Matter model resolves this and one of the known profiles incorporates the Bose-Einstein Condensate (BEC) [124]. In such a profile, the density is given as

$$\rho = \frac{\rho_c}{\lambda r} \sin(\lambda r) \quad (23)$$

where λ is related to the Compton relationship. The metric function $A(r)$ of a black hole in SFDM profile then takes the form

$$A(r) = \exp \left[-\frac{8k \sin \left(\frac{\pi r}{r_c} \right)}{\pi^2 r} \right] - \frac{2m}{r}. \quad (24)$$

Using Eq. (4), we find

$$F(u) = \frac{1}{b^2} - u^2 + 2mu^3 + \frac{8u^3 k}{\pi^2} \sin \left(\frac{\pi}{r_c u} \right), \quad (25)$$

After solving Eq. (5) iteratively, we obtain the closest approach as

$$u_o = \frac{\sin \phi}{b} + \frac{m(1 + \cos^2 \phi)}{b^2} + \frac{4r_c(b + 3m) \sin \left(\frac{\pi b}{r_c} \right) - 4\pi b m \cos \left(\frac{\pi b}{r_c} \right)}{\pi^2 b^2 r_c (b - 2m)} k. \quad (26)$$

Using this, we find ϕ_{RS} as

$$\begin{aligned} \phi_{RS} = & (\phi_{RS})_{Schw} + \frac{4k \sin \left(\frac{\pi b}{r_c} \right)}{\pi^2 b} \left[\frac{1}{\sqrt{1 - b^2 u_R^2}} + \frac{1}{\sqrt{1 - b^2 u_S^2}} \right] \\ & + \frac{4km}{\pi^2 b^2 r_c} \left\{ \frac{\left[\pi b (b^2 u_R^2 - 1) \cos \left(\frac{\pi b}{r_c} \right) - r_c (b^3 u_R^3 + 5b^2 u_R^2 - 5) \sin \left(\frac{\pi b}{r_c} \right) \right]}{(1 - b^2 u_R^2)^{3/2}} + \right. \end{aligned}$$

$$\left. \frac{\left[\pi b (b^2 u_S^2 - 1) \cos\left(\frac{\pi b}{r_c}\right) - r_c (b^3 u_S^3 + 5b^2 u_S^2 - 5) \sin\left(\frac{\pi b}{r_c}\right) \right]}{(1 - b^2 u_S^2)^{3/2}} \right\} + \mathcal{O}(m^2, k^2, m^2 k^2), \quad (27)$$

and for the last two terms in Eq. (4), we find

$$\begin{aligned} \Psi_R - \Psi_S &= (\Psi_R - \Psi_S)_{\text{Schw}} - \frac{4bk}{\pi^2} \left[\frac{u_R^2 \sin\left(\frac{\pi}{r_c u_R}\right)}{\sqrt{1 - b^2 u_R^2}} + \frac{u_S^2 \sin\left(\frac{\pi}{r_c u_S}\right)}{\sqrt{1 - b^2 u_S^2}} \right] \\ &+ \frac{8bkm}{\pi^2} \left[\frac{u_R^3 (b^2 u_R^2 - \frac{1}{2}) \sin\left(\frac{\pi}{r_c u_R}\right)}{(1 - b^2 u_R^2)^{3/2}} + \frac{u_S^3 (b^2 u_S^2 - \frac{1}{2}) \sin\left(\frac{\pi}{r_c u_S}\right)}{(1 - b^2 u_S^2)^{3/2}} \right] + \mathcal{O}(m^2, k^2, m^2 k^2). \end{aligned} \quad (28)$$

Combining the two previous equations above, the weak deflection angle with u being finite leads to

$$\begin{aligned} \hat{\alpha} &= \frac{2m}{b} \left(\sqrt{1 - b^2 u_R^2} + \sqrt{1 - b^2 u_S^2} \right) - \frac{4k}{\pi^2 b} \left\{ \frac{\left[b^2 u_R^2 \sin\left(\frac{\pi}{r_c u_R}\right) - \sin\left(\frac{\pi b}{r_c}\right) \right]}{\sqrt{1 - b^2 u_R^2}} + \frac{\left[b^2 u_S^2 \sin\left(\frac{\pi}{r_c u_S}\right) - \sin\left(\frac{\pi b}{r_c}\right) \right]}{\sqrt{1 - b^2 u_S^2}} \right\} \\ &+ \frac{4bkm}{\pi^2} \left[\frac{u_R^3 (2b^2 u_R^2 - 1) \sin\left(\frac{\pi}{r_c u_R}\right)}{(1 - b^2 u_R^2)^{3/2}} + \frac{u_S^3 (2b^2 u_S^2 - 1) \sin\left(\frac{\pi}{r_c u_S}\right)}{(1 - b^2 u_S^2)^{3/2}} \right] \\ &+ \frac{4km}{\pi^2 b^2 r_c} \left\{ \frac{\left[\pi b (b^2 u_R^2 - 1) \cos\left(\frac{\pi b}{r_c}\right) - r_c (b^3 u_R^3 + 5b^2 u_R^2 - 5) \sin\left(\frac{\pi b}{r_c}\right) \right]}{(1 - b^2 u_R^2)^{3/2}} + \right. \\ &\left. \frac{\left[\pi b (b^2 u_S^2 - 1) \cos\left(\frac{\pi b}{r_c}\right) - r_c (b^3 u_S^3 + 5b^2 u_S^2 - 5) \sin\left(\frac{\pi b}{r_c}\right) \right]}{(1 - b^2 u_S^2)^{3/2}} \right\} + \mathcal{O}(m^2, k^2, m^2 k^2). \end{aligned} \quad (29)$$

Again, if $k = 0$ and in the far approximation, $\hat{\alpha} = 4m/b$ is recovered. We notice also that u cannot be equal to zero for $\sin(\pi/r_c u)$. However, with u having a very small value, $\sin(\pi/r_c u)$ can only be somewhere between -1 and 1 . Moreover, since there is a factor of u^2 in $\sin(\pi/r_c u)$, we can safely approximate the term to zero. Therefore, Eq. (29) can be reduced to

$$\hat{\alpha} = \frac{4m}{b} + \frac{8k}{\pi^2 b} \sin\left(\frac{\pi b}{r_c}\right) + \frac{8km}{\pi^2 b^2 r_c} \left[5r_c \sin\left(\frac{\pi b}{r_c}\right) - \pi b \cos\left(\frac{\pi b}{r_c}\right) \right]. \quad (30)$$

In the SFDM profile, the parameters for Sgr. A* are the following: $\rho_c = 3.43 \times 10^7 M_\odot \text{kpc}^{-3}$ and $r_c = 15.7 \text{ kpc}$ for the core density and radius respectively, and $k = 30869m$. Fig. 3 shows how the weak deflection angle varies for different values of b/m . For the black hole only case, we can see that the increase in $\hat{\alpha}$ is very small overall, even as b/m decreases further. The same observation holds when the effect of the SFDM profile is present. Interesting behavior for the $\hat{\alpha}$ curve occurs for $b > r_c$ where fluctuation between attractive and repulsive behavior occurs. Furthermore, the amplitude of the fluctuation decreases as b/m increases, which indicates that it reaches the Schwarzschild case for very large b/m . The periodic behavior diminishes inside the core radius while we see a considerable deviation. When b is considerable small in comparison to r_c , then $\sin(\pi b/r_c) \sim \pi b/r_c$ and $\cos(\pi b/r_c) \sim 1$. Then the second term becomes $8k/\pi r_c$ which is a constant. With the parameters used herein, this constant is $\sim 1.029 \times 10^{-6}$. The third term however still depends on b/m and can be neglected due to the very tiny contribution. For this reason, the first term dominates which explains how the dark matter contribution follows the trend of the Schwarzschild case. In such a region, the only effect of the dark matter in the SFDM profile is to increase slightly the value of the weak deflection angle by some constant that depends on the black hole and dark matter parameters.

C. Effect of the URC profile on weak deflection angle by black holes

The Universal Rotation Curve profile came from the another known model called Burkert profile [125, 126]. The URC density profile is expressed as

$$\rho = \frac{\rho_c r_c^3}{(r + r_c)(r^2 + r_c^2)}. \quad (31)$$

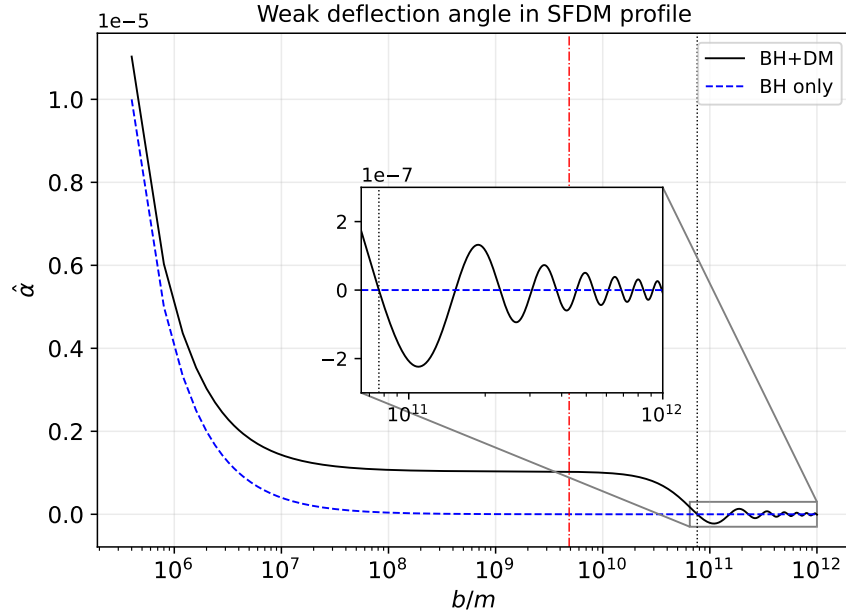


FIG. 3: Curve of the weak deflection angle in the SFDM profile for different values of the dimensionless impact parameter $b/$. The vertical dotted line is the value of the outermost core radius $r_c \sim 7.639 \times 10^{10} m$. The region below the dash-dotted vertical line is the cusp region ($\sim 4.86 \times 10^9 m$).

Taking consideration of the black hole, it was shown in [108] that $A(r)$ is somewhat complicated:

$$A(r) = \left(1 + \frac{r^2}{r_c^2}\right)^{-\frac{2\pi k(1-\frac{r}{r_c})}{r}} \left(1 + \frac{r}{r_c}\right)^{-\frac{4\pi k(1+\frac{r}{r_c})}{r}} \exp\left[\frac{4\pi k(1+\frac{r}{r_c}) \arctan\left(\frac{r}{r_c}\right)}{r}\right] - \frac{2m}{r}. \quad (32)$$

Nevertheless, it can be easily shown that when $k = 0$, the first term above is equal to 1. Calculating the orbit equation we find

$$F(u) = \frac{1}{b^2} - u^2 + 2mu^3 + 8\pi u^3 k \ln\left(\frac{1}{ur_c}\right) - \frac{4\pi k u^2}{r_c} \left[(r_c u + 1) \arctan\left(\frac{1}{r_c u}\right)\right], \quad (33)$$

and notice how we recovered the CDM contribution in the third term of the equation above despite not having Eq. (14) in Eq. (32). Now, for the sake of brevity in calculation, it is useful to omit the CDM term. After we solved iteratively, the inverse of the closest approach is found as

$$u_o = \frac{\sin \phi}{b} + \frac{m(1 + \cos^2 \phi)}{b^2} - \frac{2\pi k}{b^2 r_c (b - 2m)} \left\{ [b^2 + b(r_c + 2m) + 3r_c m] \arctan\left(\frac{b}{r_c}\right) - \frac{br_c m(b + r_c)}{(b^2 + r_c^2)} \right\}. \quad (34)$$

Now, after evaluating the two integrals in Eq. (4), we find

$$\begin{aligned} \phi_{RS} = (\phi_{RS})_{Schw+CDM} - \frac{2\pi k}{br_c} \left\{ \frac{[(b+r_c) \arctan\left(\frac{b}{r_c}\right)]}{\sqrt{1-b^2 u_R^2}} + \frac{[(b+r_c) \arctan\left(\frac{b}{r_c}\right)]}{\sqrt{1-b^2 u_S^2}} \right\} \\ + \frac{2\pi km}{b^2 r_c} \left\{ \frac{\left[\beta_R \tan^{-1}\left(\frac{b}{r_c}\right) - \frac{br_c(b+r_c)(b^2 u_R^2 - 1)}{b^2 + r_c^2} \right]}{(1-b^2 u_R^2)^{3/2}} + \frac{\left[\beta_S \tan^{-1}\left(\frac{b}{r_c}\right) - \frac{br_c(b+r_c)(b^2 u_S^2 - 1)}{b^2 + r_c^2} \right]}{(1-b^2 u_S^2)^{3/2}} \right\} + \mathcal{O}(m^2, k^2, m^2 k^2), \quad (35) \end{aligned}$$

where

$$\beta = b^3 (r_c u^3 + 4u^2) + 5b^2 r_c u^2 + b^4 u^3 - 4b - 5r_c \quad (36)$$

For $\Psi_R - \Psi_S$, we have

$$\begin{aligned} \Psi_R - \Psi_S = & (\Psi_R - \Psi_S)_{\text{Schw+CDM}} + \frac{2\pi bk}{r_c} \left[\frac{u_R(r_c u_R + 1) \arctan\left(\frac{1}{r_c u_R}\right)}{\sqrt{1 - b^2 u_R^2}} + \frac{u_S(r_c u_S + 1) \arctan\left(\frac{1}{r_c u_S}\right)}{\sqrt{1 - b^2 u_S^2}} \right] \\ & - \frac{2\pi bkm}{r_c} \left\{ \frac{u_R^2 (2b^2 u_R^2 - 1) (r_c u_R + 1) \arctan\left(\frac{1}{r_c u_R}\right)}{(1 - b^2 u_R^2)^{3/2}} + \frac{u_S^2 (2b^2 u_S^2 - 1) (r_c u_S + 1) \arctan\left(\frac{1}{r_c u_S}\right)}{(1 - b^2 u_S^2)^{3/2}} \right\} \\ & + \mathcal{O}(m^2, k^2, m^2 k^2), \end{aligned} \quad (37)$$

Combining the above equations, we find weak deflection angle in finite distance as

$$\begin{aligned} \hat{\alpha} = \hat{\alpha}_{\text{Schw+CDM}} = & \frac{2\pi bk}{r_c} \left[\frac{u_R(r_c u_R + 1) \arctan\left(\frac{1}{r_c u_R}\right)}{\sqrt{1 - b^2 u_R^2}} + \frac{u_S(r_c u_S + 1) \arctan\left(\frac{1}{r_c u_S}\right)}{\sqrt{1 - b^2 u_S^2}} \right] \\ & - \frac{2\pi bkm}{r_c} \left\{ \frac{u_R^2 (2b^2 u_R^2 - 1) (r_c u_R + 1) \arctan\left(\frac{1}{r_c u_R}\right)}{(1 - b^2 u_R^2)^{3/2}} + \frac{u_S^2 (2b^2 u_S^2 - 1) (r_c u_S + 1) \arctan\left(\frac{1}{r_c u_S}\right)}{(1 - b^2 u_S^2)^{3/2}} \right\} \\ & + \mathcal{O}(m^2, k^2, m^2 k^2). \end{aligned} \quad (38)$$

As expected, the Schwarzschild case is recovered if $k = 0$. One can not set $u = 0$ due to the divergence in ω . We say that these are only apparent divergences. Nonetheless, if u is very small, these terms can have finite values. If this is the case, then the factors u and u^2 will dominate and we can safely assume that in the far approximation, Eq. (38) should reduce to

$$\begin{aligned} \hat{\alpha} = & \frac{4m}{b} + \frac{8\pi k}{b} \ln\left(\frac{b}{r_c}\right) + \frac{8\pi km}{b^2} \left[5 \ln\left(\frac{b}{r_c}\right) + 1 \right] - \frac{4\pi k(b + r_c) \arctan\left(\frac{b}{r_c}\right)}{br_c} \\ & + \frac{4\pi km}{b^2 r_c} \frac{[br_c(b + r_c) - (4b + 5r_c) \arctan\left(\frac{b}{r_c}\right)]}{(b^2 + r_c^2)} \end{aligned} \quad (39)$$

It is interesting how we can see the emergence of the CDM profile contribution in Eq. (39). Let us use the M87 as an example [108] to demonstrate the effect of the URC profile on the weak deflection angle. The mass of the black hole at the center is given as $m = 6.5 \times 10^9 M_\odot$, while the dark matter parameters are $\rho_c = 6.9 \times 10^6 M_\odot \text{kpc}^{-3}$ and $r_c = 91.2 \text{ kpc}$ for the core density and radius respectively. We can then use $k = 805m$ for the dark matter mass. In Fig. 4, the weak deflection angle due to the black hole alone is hardly noticed for this chosen range for b/m . The overall effect of the URC profile is showing a repulsive behavior to the weak deflection angle. With $b \gg r_c$, we can see that the deviation to the Schwarzschild case is not large, though not asymptotically approaching it. We see a decrease in $\hat{\alpha}$ as b/m approaches the core radius and continues to deviate into more negative values. The deviation is considerably greater near the cusp territory compared to the CDM profile. In the figure, it is also interesting to note that when $b = r_c$, the \arctan term is equal to $\pi/4$ and the \ln term is zero. Thus, if the light ray just grazes the core radius, there is a dark matter effect unlike in the CDM and SFDM profiles.

D. Remarks on the cusp phenomenon

In this section, we comment on the possible effect of the cusp phenomenon on the weak deflection angle. Or, is there any? Looking at Fig. (1) in Ref. [34], we can see that the energy density is still finite at $r = 1 \text{ kpc}$ and it is indeed asymptotic to $+\infty$ as r approaches zero. Not taking into account the black hole, only the CDM profile produces a cusp, while the SFDM has none. With the black hole into consideration, it is reported [34] that the cusp arises in the SFDM profile as the energy density is enhanced near the black hole. We see that this cusp if it begins at $r = 1 \text{ kpc}$, it does not affect the weak deflection angle as can be gleaned from Fig. 3. The reason is that there is no peculiar deviation to the curve happening at $r = 1 \text{ kpc}$ and the increase in $\hat{\alpha}$ happens even without the dark matter SFDM profile. The weak deflection angle with the SFDM profile merely follows the same trend as the Schwarzschild case since the second term in Eq. (30) gives a constant value as b/m further decreases. In Ref. [108], it is reported that the black hole with the URC profile has no cusp phenomenon since the energy density is finite at very low values of r . We can see in Fig. 4 the behavior of the $\hat{\alpha}$ curve without the effect of the cusp. However, this behavior is also reminiscent in Fig. 2 where the cusp phenomenon exists in the CDM profile. With these observations, we cannot attribute the behavior of $\hat{\alpha}$ inside the core radius to the cusp phenomenon, but instead to the kind of astrophysical environment where the light travels. The effect of the cusp may be more evident very close to the black hole and for this reason, a study of the strong

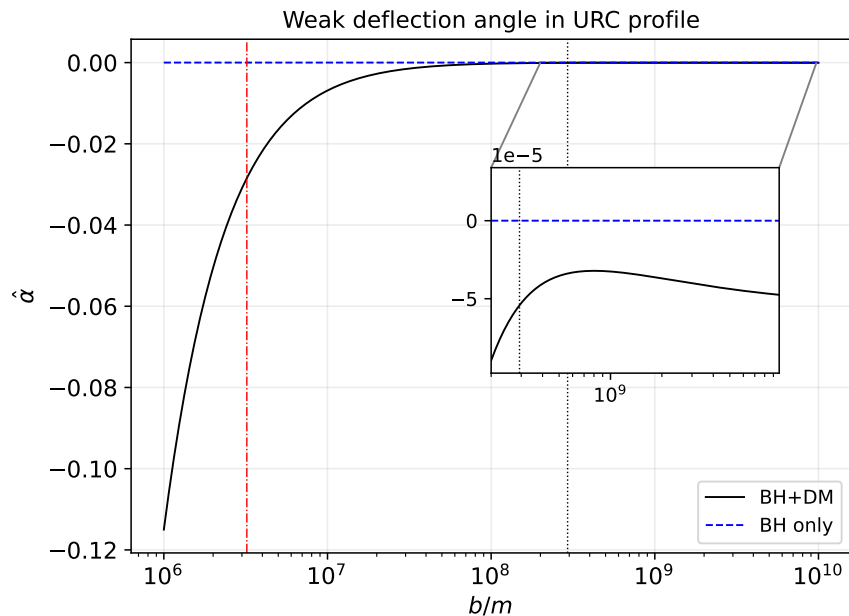


FIG. 4: Curve of the weak deflection angle in the URC profile for different values of impact parameter b . The vertical dotted line is the value of the outermost core radius $r_c \sim 2.932 \times 10^8 m$. The region below the dash-dotted vertical line is the cusp region ($\sim 3.214 \times 10^6 m$)

deflection of light is necessary to investigate such effect. Related to this, it was already reported that the horizon, ergosphere, shadow radius, and energy emission rate exhibit deviations to the standard values, and cusp effects may be one of the reasons for such deviations [34, 107, 108]. The conclusion is reasonable since these observables happen near the black hole where their fundamental properties are maintained despite being surrounded by dark matter.

III. CONCLUSION

In this work, we have obtained the weak deflection angle with finite distance for black holes surrounded by dark matter. In particular, we considered the dark matter profiles such as the CDM, SFDM, and URC profiles. With this aim, we calculated the positional angles of the source and the receiver using the method by Ishihara et. al [37], and the calculation of their longitudinal angle difference using the non-asymptotic GBT method in [45]. Using the known data and parameters for the black hole and dark matter in the Milky Way and M87 galaxies, the density profiles give a unique behavior for the weak deflection angle. According to Figs. 2 and 4, the deviation due to the CDM and URC profiles are not that evident outside the DM core radius. Noticeable deviation occurs inside the core radius as both profiles give a negative deviation which implies repulsive behavior to the null geodesic. The SFDM gives an interesting behavior to the weak deflection angle since the deviation is oscillatory outside the core radius, but follows the Schwarzschild trend inside the core radius. The behavior implies that the cusp phenomenon reported in [34] does not affect the weak deflection angle in the SFDM profile, as well as those in the CDM and URC profiles. That being said, as we compare Figs. 2-4, we can see that the weak deflection angle can give us hints on how dark matter and photons interact, at the domain near the core radius. We believe that such an analysis is better than analyzing the depths of the black hole shadow. According to the Figs. 2 - 4, the ranking of increasing difficulty to detect dark matter effect near the core radius is from URC, CDM, and SFDM profiles. Nevertheless, the Event Horizon Telescope can achieve an angular resolution of $10 \mu\text{as}$ within 345 GHz, which this is enough to observe the possible deviation of the weak deflection angle to the Schwarzschild case at the center of Sgr. A*. Another space technology that we have is the ESA GAIA mission that is capable of providing around $20 \mu\text{as} - 7 \mu\text{as}$ of angular resolution [127].

As a future research direction, it is interesting to include black hole rotation in the analysis, which is a work in progress. Another is the comparison between deflection angles of null and time-like particles. The cusp phenomenon is also interesting and

the calculation of the strong deflection angle by a black hole in dark matter profile may reveal its effect.

-
- [1] K. Schwarzschild, Sitzungsber. Preuss. Akad. Wiss. Berlin (Math. Phys.) **1916**, 189 (1916).
 - [2] The Event Horizon Telescope Collaboration, et al., *Astrophys. J. Lett.* **910**, L12 (2021).
 - [3] The Event Horizon Telescope Collaboration, et al., *Astrophys. J. Lett.* **910**, L13 (2021).
 - [4] The Event Horizon Telescope Collaboration, et al., *Astrophys. J. Lett.* **875**, L1 (2019).
 - [5] A. Einstein, *English Translation of The Foundation of the General Theory of Relativity* (Princeton University Press, 2015).
 - [6] F. Ozel, D. Psaltis, and Z. Younsi (2021), arXiv: 2111.01123.
 - [7] S. Vagnozzi, C. Bambi, and L. Visinelli, *Class. Quant. Grav.* **37**, 087001 (2020).
 - [8] A. Allahyari, M. Khodadi, S. Vagnozzi, and D. F. Mota, *JCAP* **02**, 003 (2020).
 - [9] S. Vagnozzi and L. Visinelli, *Phys. Rev. D* **100**, 024020 (2019).
 - [10] M. Guerrero, G. J. Olmo, D. Rubiera-Garcia, and D. S.-C. Gómez, *JCAP* **08**, 036 (2021).
 - [11] E. Berti et al., *Class. Quant. Grav.* **32**, 243001 (2015).
 - [12] P. V. P. Cunha and C. A. R. Herdeiro, *Gen. Rel. Grav.* **50**, 42 (2018).
 - [13] E. Barausse et al., *Gen. Rel. Grav.* **52**, 81 (2020).
 - [14] P. V. P. Cunha, E. Berti, and C. A. R. Herdeiro, *Phys. Rev. Lett.* **119**, 251102 (2017).
 - [15] H. C. D. L. Junior, P. V. P. Cunha, C. A. R. Herdeiro, and L. C. B. Crispino, *Phys. Rev. D* **104**, 044018 (2021).
 - [16] P. V. P. Cunha, N. A. Eiró, C. A. R. Herdeiro, and J. P. S. Lemos, *JCAP* **03**, 035 (2020).
 - [17] A. Abdujabbarov, B. Ahmedov, N. Dadhich, and F. Atamurotov, *Phys. Rev. D* **96**, 084017 (2017).
 - [18] B. Narzilloev, S. Shaymatov, I. Hussain, A. Abdujabbarov, B. Ahmedov, and C. Bambi, *Eur. Phys. J. C* **81**, 849 (2021).
 - [19] N. Jarosik, C. L. Bennett, J. Dunkley, et al., *Astrophys. J., Suppl. Ser.* **192**, 14 (2011).
 - [20] R. Bernabei, P. Belli, F. Cappella, et al., *Eur. Phys. J. C* **56**, 333 (2008).
 - [21] R. Bernabei, P. Belli, F. Cappella, et al., *Eur. Phys. J. C* **73**, 2648 (2013).
 - [22] R. Bernabei, P. Belli, A. Bussolotti, et al., *Nucl. Phys. At. Energy* **19**, 307 (2018).
 - [23] G. Angloher, A. Bento, C. Bucci, et al., *Eur. Phys. J. C* **76**, 25 (2016).
 - [24] C. Amole, M. Ardid, I. J. Arnquist, D. M. Asner, et al. (PICO Collaboration), *Phys. Rev. Lett.* **118**, 251301 (2017).
 - [25] D. S. Akerib, S. Alsum, H. M. Araújo, X. Bai, et al. (LUX Collaboration), *Phys. Rev. Lett.* **118**, 251302 (2017).
 - [26] S. Baum, A. K. Drukier, K. Freese, et al., *Phys. Lett. B* **803**, 135235 (2020).
 - [27] X. Hou, Z. Xu, and J. Wang, *J. Cosmol. Astropart. Phys.* **2018**, 040 (2018).
 - [28] S. Haroon, M. Jamil, K. Jusufi, et al., *Phys. Rev. D* **99**, 044015 (2019).
 - [29] R. A. Konoplya, *Phys. Lett. B* **795**, 1 (2019).
 - [30] R. C. Pantig and E. T. Rodulfo, *Chinese J. Phys.* **68**, 236 (2020).
 - [31] R. C. Pantig and E. T. Rodulfo, *Chin. J. Phys.* **66**, 691 (2020).
 - [32] R. C. Pantig, P. K. Yu, E. T. Rodulfo, and A. Övgün, *Annals of Physics* **436**, 168722 (2022).
 - [33] K. Saurabh and K. Jusufi, *Eur. Phys. J. C* **81**, 490 (2021).
 - [34] Z. Xu, X. Hou, X. Gong, et al., *J. Cosmol. Astropart. Phys.* **2018**, 038 (2018).
 - [35] G. W. Gibbons and M. C. Werner, *Class. Quantum Gravity* **25**, 235009 (2008).
 - [36] M. C. Werner, *Gen. Relativ. Gravit.* **44**, 3047 (2012).
 - [37] A. Ishihara, Y. Suzuki, T. Ono, et al., *Phys. Rev. D* **94** (2016).
 - [38] A. Ishihara, Y. Suzuki, T. Ono, and H. Asada, *Phys. Rev. D* **95**, 044017 (2017).
 - [39] T. Ono, A. Ishihara, and H. Asada, *Phys. Rev. D* **96**, 104037 (2017).
 - [40] G. Crisnejo and E. Gallo, *Phys. Rev. D* **97**, 124016 (2018).
 - [41] Z. Li and A. Övgün, *Phys. Rev. D* **101**, 024040 (2020).
 - [42] Z. Li, G. He, and T. Zhou, *Phys. Rev. D* **101**, 044001 (2020).
 - [43] Z. Li and J. Jia, *Eur. Phys. J. C* **80**, 157 (2020).
 - [44] Z. Li and T. Zhou, *Phys. Rev. D* **101**, 044043 (2020).
 - [45] Z. Li, G. Zhang, and A. Övgün, *Phys. Rev. D* **101**, 124058 (2020).
 - [46] Z. Li and T. Zhou, *Phys. Rev. D* **104**, 104044 (2021).
 - [47] Z. Li, H. Liu, and J. Jia, *Phys. Rev. D* **104**, 084027 (2021).
 - [48] M. C. Werner, *Gen. Rel. Grav.* **44**, 3047 (2012).
 - [49] G. W. Gibbons, C. A. R. Herdeiro, C. M. Warnick, and M. C. Werner, *Phys. Rev. D* **79**, 044022 (2009).
 - [50] A. Övgün, K. Jusufi, and I. Sakalli, *Phys. Rev. D* **99**, 024042 (2019).
 - [51] K. Jusufi and A. Övgün, *Phys. Rev. D* **97**, 024042 (2018).
 - [52] A. Övgün, I. Sakalli, and J. Saavedra, *JCAP* **10**, 041 (2018).
 - [53] K. Jusufi, M. C. Werner, A. Banerjee, and A. Övgün, *Phys. Rev. D* **95**, 104012 (2017).
 - [54] S. U. Islam, R. Kumar, and S. G. Ghosh, *JCAP* **09**, 030 (2020).
 - [55] A. Övgün, *Phys. Rev. D* **98**, 044033 (2018).
 - [56] K. Jusufi, A. Övgün, and A. Banerjee, *Phys. Rev. D* **96**, 084036 (2017).
 - [57] K. Jusufi, A. Övgün, J. Saavedra, Y. Vásquez, and P. A. González, *Phys. Rev. D* **97**, 124024 (2018).
 - [58] K. Jusufi, I. Sakalli, and A. Övgün, *Phys. Rev. D* **96**, 024040 (2017).

- [59] I. Sakalli and A. Ovgun, EPL **118**, 60006 (2017), 1702.04636.
- [60] R. Kumar, S. G. Ghosh, and A. Wang, Phys. Rev. D **100**, 124024 (2019).
- [61] T. Ono, A. Ishihara, and H. Asada, Phys. Rev. D **98**, 044047 (2018).
- [62] K. Jusufi and A. Övgün, Phys. Rev. D **97**, 064030 (2018).
- [63] W. Javed, R. Babar, and A. Övgün, Phys. Rev. D **99**, 084012 (2019).
- [64] H. Arakida, Gen. Rel. Grav. **50**, 48 (2018).
- [65] A. Övgün, Phys. Rev. D **99**, 104075 (2019).
- [66] G. W. Gibbons, Class. Quant. Grav. **33**, 025004 (2016).
- [67] A. Övgün, G. Gylchev, and K. Jusufi, Annals Phys. **406**, 152 (2019).
- [68] A. Övgün, K. Jusufi, and I. Sakalli, Annals Phys. **399**, 193 (2018).
- [69] T. Ono, A. Ishihara, and H. Asada, Phys. Rev. D **99**, 124030 (2019).
- [70] R. Kumar, S. G. Ghosh, and A. Wang, Phys. Rev. D **101**, 104001 (2020).
- [71] K. Jusufi, A. Övgün, A. Banerjee, and t. I. Sakalli, Eur. Phys. J. Plus **134**, 428 (2019).
- [72] K. Jusufi, N. Sarkar, F. Rahaman, A. Banerjee, and S. Hansraj, Eur. Phys. J. C **78**, 349 (2018).
- [73] A. Övgün, Universe **5**, 115 (2019).
- [74] W. Javed, j. Abbas, and A. Övgün, Phys. Rev. D **100**, 044052 (2019).
- [75] W. Javed, J. Abbas, and A. Övgün, Eur. Phys. J. C **79**, 694 (2019).
- [76] G. Crisnejo, E. Gallo, and A. Rogers, Phys. Rev. D **99**, 124001 (2019).
- [77] W. Javed, R. Babar, and A. Övgün, Phys. Rev. D **100**, 104032 (2019).
- [78] A. Övgün, I. Sakalli, and J. Saavedra, Annals Phys. **411**, 167978 (2019).
- [79] Y. Kumaran and A. Övgün, Chin. Phys. C **44**, 025101 (2020).
- [80] G. Crisnejo, E. Gallo, and J. R. Villanueva, Phys. Rev. D **100**, 044006 (2019).
- [81] K. Jusufi and A. Övgün, Int. J. Geom. Meth. Mod. Phys. **16**, 1950116 (2019).
- [82] R. Kumar, B. P. Singh, and S. G. Ghosh, Annals Phys. **420**, 168252 (2020).
- [83] A. Belhaj, M. Benali, A. El Balali, H. El Moumni, and S. E. Ennadifi, Class. Quant. Grav. **37**, 215004 (2020).
- [84] K. de Leon and I. Vega, Phys. Rev. D **99**, 124007 (2019).
- [85] T. Ono and H. Asada, Universe **5**, 218 (2019).
- [86] P. Das, R. Sk, and S. Ghosh, Eur. Phys. J. C **77**, 735 (2017).
- [87] A. Övgün and I. Sakalli, Class. Quant. Grav. **37**, 225003 (2020).
- [88] W. Javed, J. Abbas, and A. Övgün, Annals Phys. **418**, 168183 (2020).
- [89] W. Javed, A. Hamza, and A. Övgün, Phys. Rev. D **101**, 103521 (2020).
- [90] K. Takizawa, T. Ono, and H. Asada, Phys. Rev. D **101**, 104032 (2020).
- [91] W. Javed, M. B. Khadim, A. Övgün, and J. Abbas, Eur. Phys. J. Plus **135**, 314 (2020).
- [92] A. Övgün, I. Sakalli, and J. Saavedra, Chin. Phys. C **44**, 125105 (2020).
- [93] S. U. Khan and J. Ren, Phys. Dark Univ. **30**, 100644 (2020).
- [94] A. Övgün, Turk. J. Phys. **44**, 465 (2020), 2011.04423.
- [95] M. Okyay and A. Övgün (2021), arXiv: 2108.07766.
- [96] W. Javed, M. B. Khadim, and A. Övgün, Eur. Phys. J. Plus **135**, 595 (2020).
- [97] W. Javed, A. Hamza, and A. Övgün, Mod. Phys. Lett. A **35**, 2050322 (2020).
- [98] K. Takizawa, T. Ono, and H. Asada, Phys. Rev. D **102**, 064060 (2020).
- [99] Q.-M. Fu, L. Zhao, and Y.-X. Liu, Phys. Rev. D **104**, 024033 (2021).
- [100] I. D. D. Carvalho, G. Alencar, W. M. Mendes, and R. R. Landim, EPL **134**, 51001 (2021).
- [101] I. Güllü and A. Övgün, Annals Phys. **436**, 168721 (2022).
- [102] H. Arakida, JCAP **08**, 028 (2021).
- [103] W. Javed, J. Abbas, Y. Kumaran, and A. Övgün, Int. J. Geom. Meth. Mod. Phys. **18**, 2150003 (2021).
- [104] M. Halla and V. Perlick, Gen. Rel. Grav. **52**, 112 (2020).
- [105] Y. Kumaran and A. Övgün, Turk. J. Phys. **45**, 247 (2021).
- [106] W. Javed, M. B. Khadim, and A. Övgün, Int. J. Geom. Meth. Mod. Phys. **17**, 2050182 (2020).
- [107] X. Hou, Z. Xu, M. Zhou, et al., J. Cosmol. Astropart. Phys. **2018**, 015 (2018).
- [108] K. Jusufi, M. Jamil, P. Salucci, et al., Phys. Rev. D **100**, 044012 (2019).
- [109] K. Jusufi, M. Jamil, and T. Zhu, Eur. Phys. J. C **80**, 354 (2020).
- [110] K. Jusufi and K. Saurabh, Mon. Not. R. Astron. Soc. **503**, 1310 (2021).
- [111] S. Nampalliwar, S. Kumar, K. Jusufi, et al., Astrophys. J. **916**, 116 (2021).
- [112] Z. Xu, X. Gong, and S.-N. Zhang, Phys. Rev. D **101**, 024029 (2020).
- [113] Z. Xu, J. Wang, and M. Tang, J. Cosmol. Astropart. Phys. **2021**, 007 (2021).
- [114] N. Kaiser and G. Squires, Astrophys. J. **404**, 441 (1993).
- [115] R. B. Metcalf and P. Madau, Astrophys. J. **563**, 9 (2001).
- [116] A. Övgün, Universe **5**, 115 (2019).
- [117] F. Atamurotov, U. Papnoi, and K. Jusufi, Class. Quantum Gravity **39**, 025014 (2022).
- [118] M. P. Do Carmo, *Differential geometry of curves and surfaces: revised and updated second edition* (Courier Dover Publications, 2016).
- [119] W. Klingenberg, *A course in differential geometry*, vol. 51 (Springer Science & Business Media, 2013).
- [120] J. F. Navarro, C. S. Frenk, and S. D. M. White, Astrophys. J. **490**, 493 (1997).
- [121] J. F. Navarro, C. S. Frenk, and S. D. M. White, Astrophys. J. **462**, 563 (1996).
- [122] W. de Blok, Adv. Astron **2010**, 789293 (2010).

- [123] K. Nakashi, S. Kobayashi, S. Ueda, and H. Saida, *Prog. Theor. Exp. Phys.* 2019 **2019**, 073E02 (2019).
- [124] C. G. Boehmer and T. Harko, *JCAP* **06**, 025 (2007).
- [125] G. Castignani, N. Frusciante, D. Vernieri, and P. Salucci, *Natural Sci.* **4**, 265 (2012).
- [126] P. Salucci, A. Lapi, C. Tonini, G. Gentile, I. Yegorova, and U. Klein, *Mon. Not. Roy. Astron. Soc.* **378**, 41 (2007).
- [127] L. Liu and L. Prokopec, *Phys. Lett. B* **769**, 281 (2017).